Thiol Terminated 1,4-Benzenedimethanethiol Self-Assembled Monolayers on Au(111) and InP(110) from Vapor Phase

ARTICLE *in* THE JOURNAL OF PHYSICAL CHEMISTRY C · NOVEMBER 2010

Impact Factor: 4.77 · DOI: 10.1021/jp1044157

Thiol Terminated 1,4-Benzenedimethanethiol Self-Assembled Monolayers on Au(111) and InP(110) from Vapor Phase

Leonardo Salazar Alarcón,[†] Lin Chen,[‡] Vladimir A. Esaulov,[‡] Julio E. Gayone,[†] Esteban A. Sánchez,[†] and Oscar Grizzi*[,†]

Centro Atómico Bariloche-CNEA, Instituto Balseiro-UNC, CONICET, 8400 S.C. de Bariloche, Río Negro, Argentina, and Institut des Sciences Moléculaires d'Orsay, Université-Paris Sud and CNRS, Bâtiment 351, 91405 Orsay, France

Received: May 14, 2010; Revised Manuscript Received: September 7, 2010

We present results of a clean vacuum evaporative adsorption method of assembly of the conjugated dithiol molecule 1,4-benzenedimethanethiol on the surfaces of gold and indium phosphide. Measurements of direct recoil spectroscopy with time-of-flight analysis show in both cases formation of a self-assembled monolayer (SAM) with S atoms available at the SAM-vacuum interface. Investigation of the adsorption kinetics shows that a lying-down phase is formed at low exposures, which precedes the standing up SAM phase. The standing up SAM formation requires exposures of the order of a mega Langmuir. A study of the SAM stability with temperature shows that the S terminated layer survives up to ∼370 K, above this temperature a reordering of the layer takes place where S atoms are no longer available at the vacuum interface. Final desorption occurs around 450 K for Au and around 500K for InP.

1. Introduction

In recent years dithiol molecules and their self-assembly has attracted much attention because of the possibility of using them as linkers between two metallic entities.[1−13] This allows their use in molecular electronics applications[1−11] or for grafting to metallic nanoparticles as a step to building complex heterostructures.[12,13] Dithiols with phenyl units have attracted particular interest in nanoscale molecular electronics.[14−17] Indeed one of the first electrical measurements on molecules involved measuring the resistance of a 1,4-benzenedimethanethiol (BDMT; $SH-CH_2-(C_6H_4)-CH_2-SH$) molecule.[18] This was performed using a STM tip held above a gold nanoparticle deposited on top of a BDMT SAM on a gold surface. In this and other experiments one often assumes that the dithiol SAM is in fact formed of standing up molecules with one sulfur attached to the substrate and the other sulfur free at the SAM−air interface. This point, however, is much debated, and there exist considerable controversies related to the possibility of forming a layer with both sulfur ends bonded to the substrate[19−34] and also because of reports on formation of multilayers.[19,20,29]

Two approaches are normally used to prepare SAMs: from solution and from vapor phase, each having its convenience and drawbacks. In the majority of cases dithiol SAMs are grown from solution, where the role of the solvent and ambient conditions can have important effects on the film properties.[6,9,19,29−33,35−39] Growth from the dithiol vapor phase under highly controlled vacuum conditions becomes feasible when the vapor pressure is high enough at not too high temperatures, as is the case for other thiol molecules,[40] allowing the formation of SAMs without ambient effects such as photo-oxidation.[33,35] This method allows the use of highly reactive substrates including semiconductors, which can undergo controlled vacuum preparation before SAM assembly. The vapor method approach has been used less frequently for dithiol SAMs,[9,21,27,28] for which both lying down or mixed phases were reported. In particular, Pasquali et al.[21] combined several spectroscopies to study the adsorption of BDMT on gold from the vapor phase up to around 50 kL, finding that at the highest exposures a large fraction of the molecules were in a standing up configuration. In this paper we present a comparative study of the vapor phase assembly of BDMT on gold and a semiconductor, indium phosphide, and use a nondestructive ion based technique (direct-recoiling spectroscopy with time-of-flight analysis, TOF-DRS)[41] to determine the presence of S atoms at the film vacuum interface and the stability of the SAM layer with annealing temperature. This ion based technique is particularly adequate to study organic films of nanometric thickness because it is extremely sensitive to top surface atoms, produces negligible damage to the organic layer, and can detect directly all atoms including H which is not detected by most other spectroscopies.[41−43] With this technique we are able to follow the adsorption kinetics in situ, from a lying down phase at low exposures to a high exposure phase of standing up molecules. The exposure condition and dose to obtain this phase is delineated. TOF-DRS spectra taken at different sample temperatures provide information on the changes taking place at the surface and the products remaining after desorption.

2. Experimental Details

The experiments were carried on a previously described[42] UHV chamber with facilities for in situ sample preparation and characterization that is connected to a 1−100 keV ion accelerator. The Au(111) and InP(110) single crystals were prepared by cycles of Ar sputtering and annealing (at 1 keV/720 K and 0.5 keV/650 K, respectively) and characterized in both cleanliness and surface order by TOF-DRS. In TOF-DRS, the sample is bombarded by a pulsed beam of keV Ar^+ or Kr^+ ions at different incidence angles (measured with respect to the surface plane). A time-of-flight analysis of the primary recoiled target

* Corresponding author. E-mail: grizzi@cab.cnea.gov.ar. Phone: 54 2944 445220. Fax: 54 2944 445299.
[†] Instituto Balseiro-UNC.
[‡] Université-Paris Sud and CNRS.

10.1021/jp1044157
Published on Web 11/09/2010

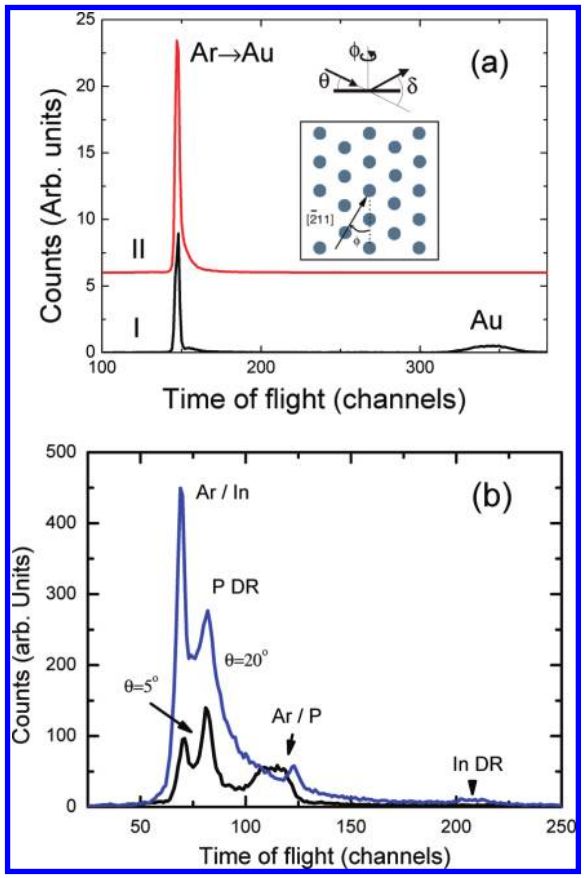

Figure 1. (a) Characteristic time-of-flight spectra for 4.2 keV Ar^+ scattering on Au(111) along two different azimuths. Spectrum II was taken along $\phi = 30°$ and I along $\phi = 0°$. Note the absence of the Au recoil peak for the compact azimuth due to shadowing effects. The insets show schematics of the scattering geometry and of the top view of the Au crystal. (b) TOF-DRS spectra from InP(110) taken at 5° and at 20° incidence angles.

atoms (named direct recoils DR) and the scattered Ar atoms is then performed by using a detector (Channel electron multiplier) placed at the end of a 0.96 m long time-of-flight tube set at 45° with respect to the incidence beam direction. Both neutral and ion scattered particles are detected with similar sensitivity thus avoiding uncertainties due to the electron exchange processes that can take place at the surface. Figure 1(a) shows typical spectra for Au(111) taken along two different azimuthal orientations ϕ (see inset of figure 1(a) for angle definition). Spectrum I, taken at 20° incidence (θ polar angle), is comprised of mainly two peaks corresponding to Ar scattered from Au and recoiled Au atoms. The assignment of peaks in these spectra is based on simple calculation of collision kinematics.[41] The absence of C and H structures at the left side of the Ar scattering peak indicates a very clean surface (typical sensitivity 1% ML[41]). In keV ion-surface scattering, a compact surface like the Au(111) presents strong shadowing effects during both the incoming and outgoing trajectory, which appear as strong variations in the intensity of the TOF spectral features with incidence and observation angles.[41] As an example, in spectrum II, taken along the more compact direction, the Au recoil peak is absent. In fact, due to shadowing effects, the Au recoil peak cannot be observed except along directions where the distance between adjacent atoms along the ion trajectory is large (as for spectrum I of Figure 1a taken along the [−211] surface channel), and even in this case the Au peak is affected by strong focusing. A complete analysis of these dependences gives information on the atomic surface structure. As an example for InP(110) we observe in figure 1b that at grazing incidence ($\theta = 5°$) P related features dominate in agreement with the surface relaxed geometry where the P atoms are lying higher than In atoms. At large angles ($\theta = 20°$), the In related features become more prominent due to focusing and a higher scattering cross section. For other azimuths (keeping the same polar angle of incidence), the relative intensity of the structures can change dramatically. The InP surface is more open than the Au surface, and hence, it is possible to find azimuthal directions where DRs can be measured without focusing or shadowing effects.

The solid BDMT (from Sigma Aldrich Argentina, 98%), initially contained in a vacuum sealed glass tube, is degassed and heated to about 85 °C and the vapors are introduced into the UHV chamber via a leak valve and a 1/4″ stainless steel tube running from the leak valve to 3 cm from the sample, all maintained at the same temperature and saturated with the BDMT vapor. For characterization of the adsorption kinetics, after each exposure a TOF-DRS spectrum is taken immediately in situ. Once the layers are grown we proceed to heat the surface and to characterize it by TOF-DRS in order to study the dependence of the top layer composition versus annealing temperature and the products remaining at the surface after the thermal desorption. The low intensity of the pulsed beam ($<10^{-12}$ A for a few minutes) results in negligible damage of the adsorbed layer,[42] allowing us to follow in great detail the adsorption kinetics from sub-Langmuir to mega-Langmuir exposures and the layer composition versus sample temperature. The absence of damage is checked by taking many spectra (more than 10) after a particular exposure and verifying that all spectra look alike; that is, there is no change in the spectral features, in both the general shape and in the ratio of DR intensities. In order to observe changes induced by the ion bombardment we need to switch to continuous beam mode and increase the ion current more than 2 orders of magnitude.

3. Results and Discussion

3.1. Adsorption of BDMT on Au(111). TOF spectra for the clean Au(111) surface and after various exposures to BDMT are shown in Figure 2 for two typical incidence angles, 20° and 5°, together with the plot of the intensities of the relevant features in the spectra versus exposure. At grazing angles (Figure 2b) the technique is more sensitive to top surface atoms, whereas at 20° (Figure 2a) the heavy ions can penetrate the layer providing information also on the atoms lying below the top ones.[41−43] These angles are not critical, i.e., measurements in the range of 3° to 6° give similar results; here the shadowing cones cast by the combination of projectile and target atoms lie more parallel to the surface thus decreasing projectile penetration. The highest film penetration is obtained at larger incident angles, however, since the scattering angle is 45°, if we increase the incident angle beyond 20° or 25° the outgoing trajectory starts to be more grazing and blocking effects prevent ejection of the underlying atoms. When BDMT is introduced, in the initial absorption stages, the spectra of the exposed surface show well-defined peaks corresponding to H DR and C DR in addition to the scattered Ar and Au DR (Figure 2(a)). The H and C DR peaks are superimposed on a broader structure coming from surface recoils, i.e., recoils going first toward the surface and then reflected back (inset in Figure 2a). With increasing exposures the scattered Ar peak decreases and becomes broader with a long tail due to multiple scattering involving both lighter molecule atoms and substrate atoms. The evolution of the intensities of these peaks (obtained as the peak area after background subtraction, Supporting Information) shows a fast

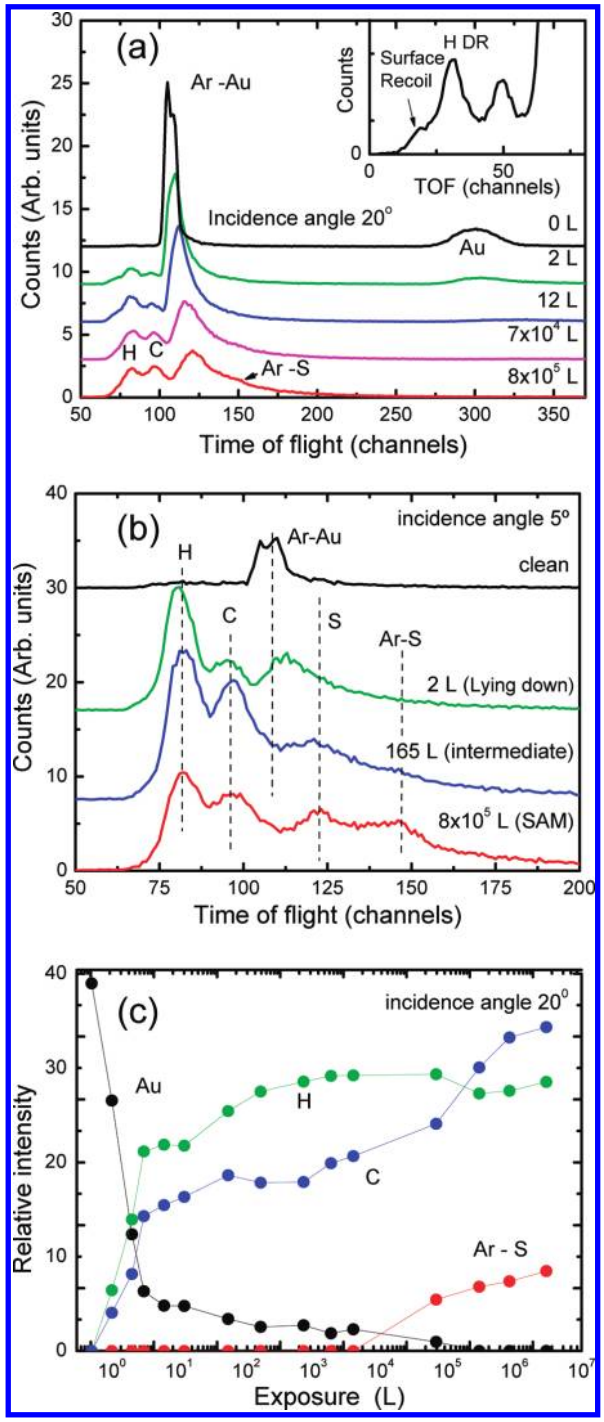

Figure 2. Characteristic time-of-flight spectra for 4.2 keV Ar^+ scattering on Au(111) exposed to different doses of BDMT. (a) 20° incidence angle and (b) 5° incidence angle. (c) Intensity of recoiled H, C, and Au versus exposure, together with the intensity of Ar scattered from S.

initial drop of the Au DR peak and an associated increase in the intensity of the H and C DR peaks (Figure 2c). The initial increase is very rapid up to ~5 L, indicating a high initial sticking coefficient, and then the intensities keep changing more slowly up to a few thousand L where additional changes appear in both the relative intensities and in the shape of the spectra.

In the only prior investigation of vapor phase absorption of BDMT on gold known to us,[21] it was concluded that the initial stage of adsorption corresponds to molecules lying on the surface with both sulfur ends bonded to gold. This assertion was based on NEXAFS measurements and XPS measurements that showed

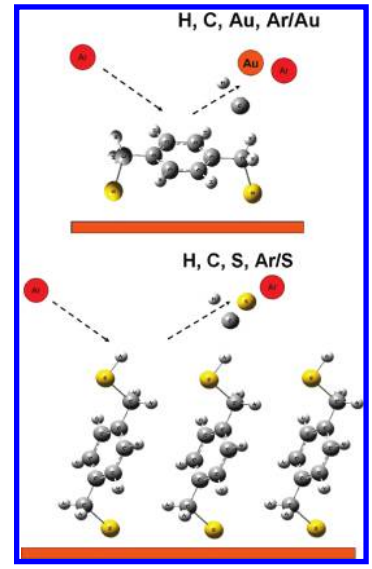

Figure 3. Schematic diagram of the scattering geometry for molecular configurations parallel to the surface (top figure) and standing-up with exposed S to the vacuum interface (lower figure).

only the existence of a peak corresponding to a thiolate. At higher coverages existence of a mixed phase was reported. Our TOF spectra for low exposures (up to about 100 L) agree with the assumption of an initially lying down phase, where both S atoms are lying closer to the surface than the C atoms. For this molecule orientation, the high surface sensitivity of the technique allows the clear observation of H and C but precludes observation of the S atoms attached to Au due to the shadowing cast by the C atoms lying close but slightly higher than S. This thin layer does not impede however that a fraction of the incident Ar ions reach the substrate, and hence a contribution of scattered Ar and Au recoils is observed in the spectra. The contribution from Ar scattered off Au through multiple collisions provides some information about the thickness of the organic layer lying on top; this will be discussed in more detail below. The general evolution of the TOF-DRS spectra is similar to the case of single alkane-thiols assembled on Ag and on Au.[42,43] The observation of the surface recoiling process also agrees with this assumption. These types of processes are better observed for light atoms adsorbed very close to heavy substrates.[41] In our case, H associated structures like the one shown in the inset of Figure 1 are characteristic of molecules lying parallel to the surface plane.[42,43] Above 10 kL the spectra show again a rapid change, with a higher attenuation of the Au DR and Ar scattering on Au as well as the appearance of two new structures in the grazing spectra assigned to recoiled sulfur atoms (S DR) and scattering of Ar on S. The observation of these two structures can occur only if sulfur is exposed in the film-vacuum interface. The onset for observation of the two S related structures is in agreement with the results from Pasquali et al.[21] and can therefore be considered as the fingerprint for the initiation of the standing up phase, with S atoms lying at the SAM/vacuum interface. The formation of a circa one nm thick standing BDMT layer[37] efficiently shields off the gold surface and therefore, at grazing incidence, the scattering and recoiling events take place at the outer part of the SAM. The scattering geometry in each case is illustrated schematically in Figure 3, where we consider a molecule orientation as proposed in ref.[21] These schematics should be considered qualitatively for exemplifying the absence and presence of S in the TOF spectra at low and high exposures, respectively, but not as a detailed adsorption model, which still remains unknown. At intermediate exposures, the layer must

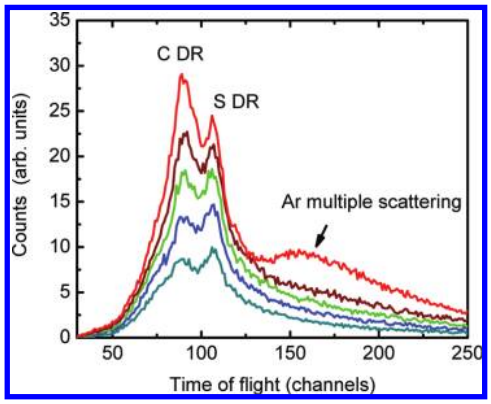

Figure 4. Time of flight spectra for 3.1 keV Kr^+ scattering off Au(111) covered with a monolayer of BDMT at different incidence angles, 8° (bottom), 10°, 12°, 14°, and 20° (top).

be mixed and so we continue to see some Ar scattering through the thin lying down regions and the mixed domains. At about 100 kL the sulfur recoil peak is already intense and sharp, but the peak corresponding to Ar scattering on S continues to increase in intensity. At very high exposures, of the order of a mega Langmuir, the intensity of both peaks corresponding to sulfur is large and their growth saturates. The H and C recoil peak change in their relative intensity and both become broader (due to recoiling from different heights). Concomitantly the recoiling gold peak strongly decreases in intensity and at the highest exposures is no longer observed (Figure 2c). These observations suggest the disappearance of large domains of lying down phase and formation of a standing up phase of BDMT on gold. The absorption curve for BDMT becomes qualitatively similar to that reported previously for hexanethiol[42] except that the dose required to saturate the SAM phase is almost 1 order of magnitude higher.

Further evidence of the exposed S at the film−vacuum interface can be accessed from a study of the saturated surface with projectiles at different angles. This is shown in Figure 4 for 3.1 keV Kr ions hitting the surface at different incident angles. Kr ions, being heavier than Ar ions, have larger shadowing cones and require slightly higher incident angles to focus on a specific layer. In this case, the S DR appears at the left side of the scattering peak and thus becomes better identified, i.e., not buried in the tail of the scattering peak as is the case for Ar projectiles at high incident angles. On the other hand, H atoms are recoiled with too low energies and are detected by the channeltron with much lower sensitivity (and are hardly observed). The C and S DR cross sections are within 25% and the efficiency to detect them very similar. Even though there are more C atoms than S atoms in the molecule (a factor 4) one can observe that the S peak dominates at the lower angles (8° spectrum), whereas the C DR peak becomes stronger at the higher angles, when the Kr ions penetrate the BDMT layer allowing more C layers (from the same molecule) to be sampled. This is a clear indication that for the BDMT saturated surface the S atoms are sitting higher than the C atoms. The absence of Au recoils or of Kr scattering from Au is also an indication that most of the surface should be covered with a standing up phase. The set of spectra shown in Figure 4 were taken a day after the adsorption, with the sample maintained at room temperature in vacuum. Spectra taken immediately following the exposure present the same characteristics, which shows the high stability of the BDMT layer when maintained in vacuum.

Another question addressed in this work is whether the organic layer formed corresponds to a single monolayer or a multilayer. Normally, some information regarding the thickness of the layer can be obtained through ellipsometry or by calibration of XPS substrate signals. Here we use the fact that Ar ions can penetrate a thin and light layer and be scattered off the underlying Au surface through multiple collisions. These types of events appear in the TOF-DRS spectra as an Ar peak broader and shifted toward lower energies (higher TOFs), which decreases when the thickness of the layer on top increases. We have simulated these multiple scattering events with the SRIM 2006 code,[44] which is known to reproduce well the penetration of ions in amorphous solids. This code cannot reproduce accurately single events affected by focusing or shadowing in single crystals, like the double focusing seen from the clean surface at some specific azimuthal directions, nevertheless its application here to obtain some hints about single versus multiple layer formation is justified by the fact that the Ar−Au scattering event becomes a multiple scattering process when the BDMT layer is on top. Different types of layers were simulated on top of an amorphous Au substrate. First, an amorphous 5 Å layer with the atomic density of the lying down phase was considered. This layer was divided in two sublayers, the first one formed with S atoms on top of the Au surface and the second one with H and C atoms exposed to the vacuum interface as shown in the top panel of Figure 3. Then, a 10 Å layer divided into three sublayers corresponding to one methanethiol sublayer right on top of the Au substrate, followed by the benzene sublayer and another sublayer of methanethiol on top (resembling the SAM phase shown in the lower panel of Figure 3, i.e., with the same atomic density in each sublayer), a third layer composed of one lying down plus one standing up SAM (∼15 Å), and finally two SAM layers (∼20 Å). The scattering geometry used in the simulation is the same as that of the experiment, i.e., the same incident and observation angle. The simulated Ar scattering peak for the first three cases is shown in Figure 5 together with the corresponding experimental contribution of Ar scattering (obtained after subtraction of the recoiling peaks and a smooth background). No broadening due to experimental resolution was included in the simulation. The simulation is normalized to the Ar contribution from the clean surface.

We observe from Figure 5 that what we considered to be the lying down phase spectrum agrees better (in relative intensity and TOF distribution) with the simulated Ar scattering with a 5 Å layer (lying down). The experimental spectrum at saturation also agrees better with the simulation for a 10 Å layer. A double layer (assuming one lying down and another standing up, i.e., 15 Å) gives an Ar contribution that is too small and shifted too much toward higher TOF, in disagreement with the experimental observation. A 20 Å layer (not shown) gives a contribution that is even in more disagreement, it essentially produces no contribution from Ar scattering off Au.

3.2. Adsorption of BDMT on InP(110). Adsorption from the gas phase might be particularly useful in more reactive surfaces where preparation in vacuum would help to preclude substrate contamination. However, it is not evident that BDMT will undergo the transition to a standing up configuration in these cases. In the following we will show that for the surface of a compound semiconductor (InP(110)) BDMT starts binding to the surface in an initially lying down configuration (as in Au) and that for sufficiently high doses it also undergoes a transition where S atoms are exposed to the vacuum interface.

Thiol assembly on GaAs[6,8,9,43,45−50] has been investigated more frequently than on InP.[51−58] Investigation of dithiols assembly on such substrates is fairly rare and mainly from solution.[9,59,60]

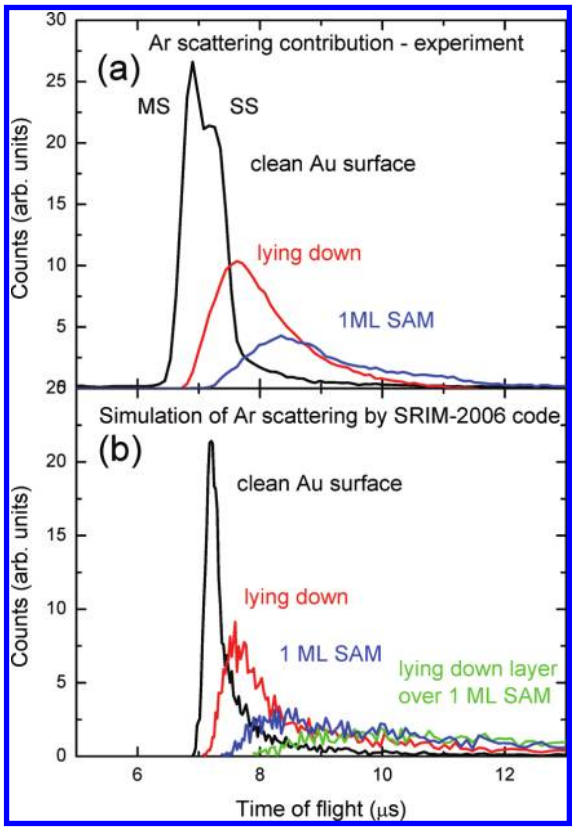

Figure 5. (a) Ar scattering contribution measured for 4.2 keV scattering from clean Au for exposures of ~165 L (lying down phase) and ~8×10^5 L (standing up phase). The recoil contribution was subtracted from these spectra. (b) Simulations of the Ar scattering spectra with SRIM 2006 code[44] for amorphous Au and for Au covered with 5 Å (lying down), 10 Å (standing up), and 15 Å (lying down plus standing up) BDMT layers.

Figure 6 shows TOF spectra for various exposures to BDMT for 5° and 20° incidence angle (panels a and b, respectively) together with the intensity of the main peaks obtained from a series of spectra measured at 20° (panel c). The initial spectrum on the clean InP substrate is comprised of peaks corresponding to Ar ions scattered from In and P and recoiled In and P atoms (In DR and P DR, respectively). Similarly to the case of GaAs(110),[61,62] and as mentioned in the experimental section, In recoils can only be seen at high incidence angles or at specific azimuthal orientations. Dosing with BDMT results in a rapid appearance of peaks related to H and C and leads to an attenuation of the substrate related structures. The Ar scattering peak becomes attenuated, broader and shifted to higher TOF. The absorption kinetics has some similarities to gold, i.e., initially the S related features are not seen, although in this case the proximity with the P peaks reduces the sensitivity. This condition is maintained up to about 1000−10 000 L where we start to see the growth of small structures associated with S DR and Ar scattering on S. The structures become very prominent at exposures of hundred thousand Langmuirs, where a strong S DR peak can be seen as in the case of gold as well as the Ar scattering on S. Note that the S related structures are comparable in magnitude to the P ones in the clean surface, except that the latter are better defined. This high S intensity and the full disappearance of substrate related features indicate that also in InP the film undergoes a transition toward a molecule orientation where S is clearly exposed in the vacuum interface. The fact that the S features are less defined than the P ones for the clean surface may be due to a combination of phenomena:

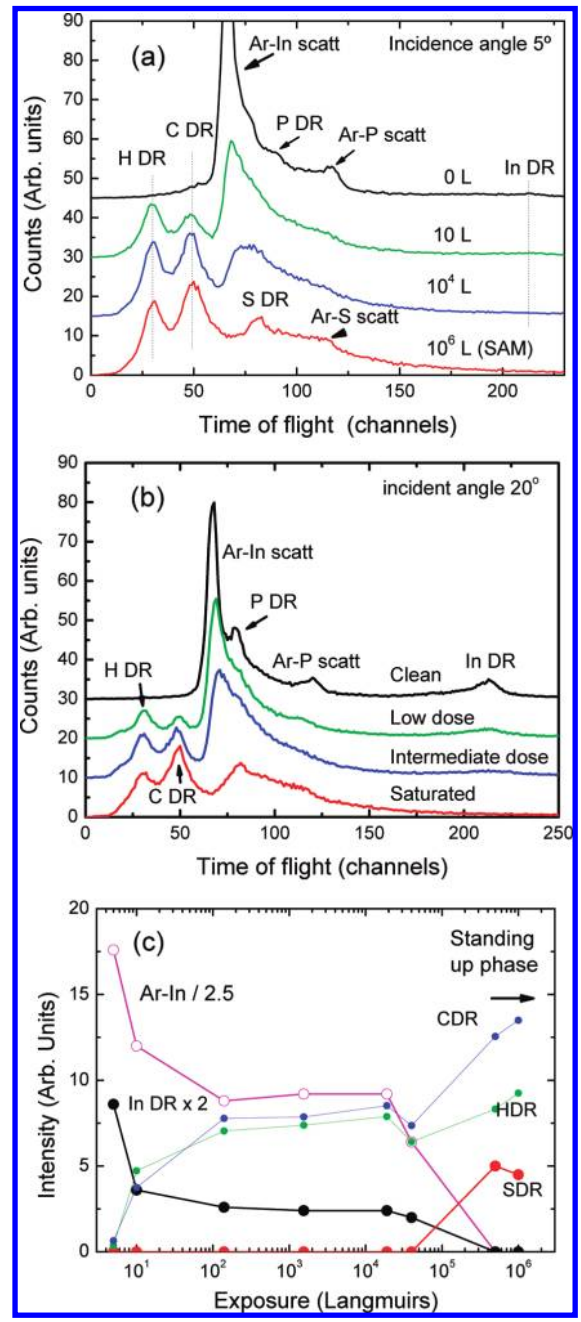

Figure 6. Characteristic time-of-flight spectra for 4.2 keV Ar^+ scattering off InP(110) exposed to different doses of BDMT at 5° (a) and at 20° (b) incidence angle. (c) Intensity of recoiled H, C, S, and In versus exposure obtained from spectra recorded at 20°, together with the intensity of Ar scattered from In.

1) for S the DR and Ar scattering peaks are closer to each other than for P, 2) the substrate is very well ordered along the whole surface while the organic film may not be so well ordered, and 3) the large molecule vibrations may affect the recoil and scattering peak shapes. Detailed comparison of the spectra for full coverage in Au and in InP shows differences in the relative intensities of the characteristic peaks and also differences in the dependence of these structures with incident and azimuthal angle. For example, the final H/C ratio is different for Au than for InP, the same happens with the C/S ratio, or the intensity of the Ar scattering peak at large incident angles. These specific scattering features indicate that the films are not identical in each surface, however other type of spectroscopies are necessary to identify these differences in the film structure.

3.3. Stability of the BDMT Layer with Sample Temperature. Some stability of the organic layer above room temperature is desirable in order to withstand or at least facilitate further processing in the case of device fabrication. As an example, in GaAs(110), we have observed before that hexanethiol layers formed from the vapor phase present a desorption peak slightly above room temperature.[43] Furthermore, the organic layer can undergo several phase transformations before desorption, not only from standing up to lying down configurations but also between different molecular orientations within the standing up configuration, as has been observed by STM measurements for single-chain thiols on Au.[63,64] Determining these phases or configurations in full detail is a very difficult task, up to now only attempted for the more standard case of thiols on some noble metals. TOF-DRS measurements can be performed in situ with many spectra taken as a function of sample temperature without imparting a detectable damage to the layer. In the following results, the typical rate for temperature variation is around 3 K/min. A change in the peak shapes or intensities indicates that some sort of modification has occurred in the layer. This mass spectroscopy technique is complementary to other thermal desorption techniques, because it samples what remains at the surface, with sensitivity to small changes at the outermost surface layer. Our TOF-DRS results are exemplified by some characteristic spectra shown in Figure 7 for the InP sample (a and b) and for Au (c). Up to ~370 K, the spectra taken at 5° incidence retain the features of a S terminated surface, showing, besides the H and C DR peaks, both the sharp S DR and the Ar scattering on S peaks that are the fingerprints of the standing up configuration. Some changes in the intensity of the grazing spectra are seen within this temperature range, probably indicating some reordering in the molecule layer. At 20° incidence there are no detectable changes in the spectra within this temperature range. Around 370 K, a clear and reproducible change is detected at grazing incidence, the intensity of the Ar scattering on S decreases very fast and the sharp S DR changes into a broader peak shifted toward the position of the P DR and of the Ar scattering from both molecule and surbstrate (Figure 7a). This behavior has been reproduced in several adsorption/desorption measurements followed with both Ar and Kr projectiles. We interpret this as a transition toward a lying down phase, or at least a configuration where S is no longer available at the top. Some molecule desorption may accompany this process. The same behavior of disappearance of S at the top of the layer is also seen in Au, at the same transition temperature. The new configuration is stable up to near 450 K, where a clear desorption of the molecule starts to take place. We observe this transition as a strong and simultaneous decrease in the H and C DR peaks and the appearance of the Ar scattering from clean substrate regions (Figure 7b) together with the other substrate features. The final desorption takes place around 500 K for InP and around 450 K for Au. A similar difference has been found for the desorption of alkanethiols from Au and from GaAs,[43] which suggests a stronger interaction between the S and the semiconductor. In the case of GaAs, a considerable higher amount of S is left at the surface when compared to the Au case. Some variation in the desorption temperature is observed for nonsaturated BDMT layers, being lower for lower coverages. Basically no C or H is left at the surface in the case of InP while some C, H and S does remains at the Au surface that cannot be removed by annealing at higher temperatures (Figure 7c). In the case of InP, due to the proximity of the S and P DR peaks, it is not possible to determine if some S remains after annealing. In the case of alkanethiols and dithiols there is no C or H remaining at the surface after annealing, only in the case of BDMT and some perylene based molecules we have found C and H after annealing.[65] The fact that H and C remain on Au but not on InP could be related to differences in charge transfer leading to dissociation of BDMT on Au, but this point needs further theoretical investigation.

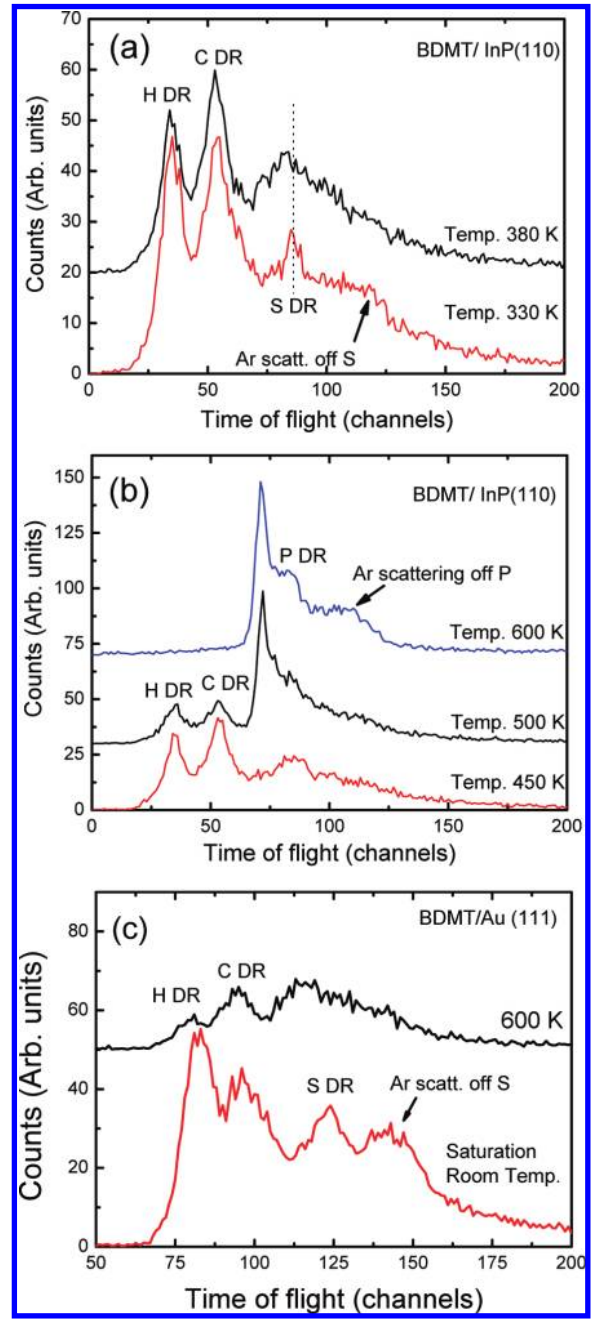

Figure 7. Time of flight spectra for 4.2 keV Ar^+ scattering from BDMT fully covered InP(110) at 5° incidence angle for temperatures near the standing up−lying down phase transition (a) and around the film desorption temperature (b). (c) Time of flight spectra for BDMT/Au(111) after saturation (room temperature) and after annealing to 600 K.

4. Conclusions

In summary, our results of evaporative adsorption of the conjugated dithiol molecule BDMT on gold and indium phosphide clearly shows formation of a SAM (one monolayer) with S atoms available at the SAM vacuum interface for binding

to e.g. metal electrodes. In both cases optimal conditions for SAM formation require high exposures of the order of a mega Langmuir. These layers are stable up to near 370 K where a transition takes place that removes the S atoms from the top of the layer, most probably implying a standing up to lying down transition. The new layer remains at the surface up to ~450 K in InP and 400 K in Au, where molecule desorption begins, and ends approximately 50 K higher. The vapor assembly method for BDMT is then an alternative to solvent assembly and can be applied to semiconductor surfaces.

Acknowledgment. This work was supported by the ECOS Sud MINCyT program A07E01. We acknowledge fruitful discussions with Drs. R. Salvarezza and B. Blum and supporting funds from MINCyT (PICT 06-715), the Argentine Nanoscience Network PAE (22708 and 22711), CONICET (PIP 112-200801-00958), and UNC (06/C323 and 06/C317).

Supporting Information Available: Additional information about adsorption sequence, including additional figures. This material is available free of charge via the Internet at http://pubs.acs.org.

References and Notes

(1) Käshammer, J.; Wohlfart, P.; WeiB, J.; Winter, C.; Fisher, R.; Mittler-Neher, S. *Opt. Mater.* **1998**, *9*, 406–410.
(2) Rieley, H.; Kendall, G. K.; Zemicael, F. W.; Smith, T. L.; Yang, S. *Langmuir* **1998**, *14*, 5147–5153.
(3) Aliganda, A. K. A.; Lieberwirth, I.; Glasser, G.; Duwez, A.-S.; Sun, Y.; Mittler, S. *Org. Electron.* **2007**, *8*, 161–174.
(4) Sakotsubo, Y.; Ohgi, T.; Fujita, D.; Ootuka, Y. *Phys. E* **2005**, *29*, 601–605.
(5) Liang, J.; Rosa, L. G.; Scoles, G. *J. Phys. Chem. C* **2007**, *111*, 17275–17284.
(6) Krapchetov, D. A.; Hong, M.; Jen, A. K. Y.; Fischer, D. A.; Loo, Y.-L. *Langmuir* **2008**, *24*, 851–856.
(7) Fahlman, M.; Salaneck, W. R. *Surf. Sci.* **2002**, *500*, 904–922.
(8) Krapchetov, D. A.; Hong, M.; Jen, A. K. Y.; Fischer, D. A.; Loo, Y.-L. *Langmuir* **2005**, *21*, 5887–5893.
(9) Loo, Y.-L.; Lang, D. V.; Rogers, J. A.; Hsu, J. W. P. *Nano Lett.* **2003**, *3*, 913.
(10) Li, W.; Kavanagh, K. L.; Matzke, C. M.; Talin, A. A.; Léonard, F.; Faleev, S.; Hsu, J. W. P. *J. Phys. Chem. B* **2005**, *109*, 6252–6256.
(11) Hsu, J. W. P.; Lang, D. V.; West, K. W.; Loo, Y.-L.; Halls, M. D.; Raghavachari, K. *J. Phys. Chem B* **2005**, *109*, 5719–5723.
(12) Pethkar, S.; Aslam, M.; Mulla, I. S.; Ganeshan, P.; Vijayamohanan, K. *J. Mater. Chem.* **2001**, *11*, 1710–1714.
(13) Sarathy, K. V.; Thomas, P. J.; Kulkarni, G. U.; Rao, C. N. R. *J. Phys. Chem. B* **1999**, *103*, 399–401.
(14) Sun, Q.; Selloni, A.; Scoles, G. *J. Phys. Chem. B* **2006**, *110*, 3493–3498.
(15) Coropceanu, V.; Cornil, J.; da Silva Filho, D. A.; Olivier, Y.; Silbey, R.; Brédas, J.-L. *Chem. Rev.* **2007**, *107*, 926–952.
(16) Mirkin, C. A.; Ratner, M. A. *Annu. Rev. Phys. Chem.* **1992**, *43*, 719–754.
(17) Reed, M. A.; Zhou, C.; Muller, C. J.; Burgin, T. P.; Tour, J. M. *Science* **1997**, *278*, 252.
(18) Andres, R. P.; Bein, T.; Dorogi, M.; Feng, S.; Henderson, J. I.; Kubiak, C. P.; Mahoney, W.; Osifchin, R. G.; Reifenberger, R. *Science* **1996**, 1323–1325.
(19) Pugmire, D. L.; Tarlov, M. J.; Van Zee, R. D. *Langmuir* **2003**, *19* (9), 3720–3726.
(20) Pasquali, L.; Terzi, F.; Zanardi, C.; Pigani, L.; Seeber, R.; Paolicelli, G.; Suturin, S. M.; Mahne, N.; Nannarone, S. *Surf. Sci.* **2007**, *601* (5), 1419–1427.
(21) Pasquali, L.; Terzi, F.; Seeber, R.; Doyle, B. P.; Nannarone, S. *J. Chem. Phy.* **2008**, *173* (1−3), 134711.
(22) Joo, S. W.; Han, S. W.; Kim, K. *J. Phys. Chem. B* **1999**, *103* (49), 10831–10837.
(23) Rifai, S.; Morin, M. *J. Electroanal. Chem.* **2003**, *550−551*, 277–289.
(24) Qu, D.; Uosaki, K. *J. Phys. Chem. B* **2006**, *110* (35), 17570–17577.
(25) Silien, C.; Dreesen, L.; Cecchet, F.; Thiry, P. A.; Peremans, A. *J. Phys. Chem. C* **2007**, 6357–6364.
(26) Venkataramanan, M.; Ma, S.; Pradeep, T. *J. Colloid Interface Sci.* **1999**, *216* (1), 134–142.
(27) Kobayashi, K.; Horiuchi, T.; Yamada, H.; Matsushige, K. *Thin Solid Films* **1998**, *331*, 210–215.
(28) Kobayashi, K.; Umemura, J.; Horiuchi, T.; Yamada, H.; Matsushige, K. *Jpn. J. Appl. Phys.* **1998**, *37*, L297–L299.
(29) Kohli, P.; Taylor, K. K.; Harris, J. J.; Blanchard, G. J. *J. Am. Chem. Soc.* **1998**, *120*, 11962–11968.
(30) Carot, M. L.; Esplandiu, M. J.; Cometto, F. P.; Patrito, E. M.; Macagno, V. A. *J. Electroanal. Chem.* **2005**, *579*, 13–23.
(31) Käshammer, J.; Wohlfart, P.; Weiss, J.; Winter, C.; Fischer, R.; Mittler-Neher, S. *Opt. Mater.* **1998**, *9*, 406–410.
(32) Esplandiu, M. J.; Carot, M. L.; Cometto, F. P.; Macagno, V. A.; Patrito, E. M. *Surf. Sci.* **2006**, *600*, 155–172.
(33) Rieley, H.; Kendall, G. K.; Zemicael, F. W.; Smith, T. L.; Yang, S. *Langmuir* **1998**, *14*, 5147–5153.
(34) Leung, T. Y. B.; Gerstenberg, M. C.; Lavrich, D. J.; Scoles, G.; Schreiber, F.; Poirier, G. E. *Langmuir* **2000**, *16*, 549–561.
(35) Hamoudi, H.; Guo, Z. A.; Prato, M.; Dablemont, C.; Zheng, W. Q.; Bourguignon, B.; Canepa, M.; Esaulov, V. A. *Phys. Chem. Chem. Phys.* **2008**, *10*, 6836–6841.
(36) Daza Milone, M. A.; Hamoudi, H.; Rodríguez, L. M.; Rubert, A.; Benitez, G. A.; Vela, M. E.; Salvarezza, R. C.; Gayone, J. E.; Sánchez, E. A.; Grizzi, O.; Dablemont, C.; Esaulov, V. A. *Langmuir* **2009**, *25*, 12945–12953.
(37) Hamoudi, H.; Prato, M.; Dablemont, C.; Cavalleri, O.; Canepa, M.; Esaulov, V. A. *Langmuir* **2010**, in press.
(38) Lau, K. H. A.; Huang, C.; Yakovlev, N.; Chen, Z. K.; O'Shea, S. J. *Langmuir* **2006**, *22,7*, 2968–2971.
(39) Niklewski, A.; Azzam, W.; Strunskus, T.; Fischer, W. A.; Wöll, Ch. *Langmuir* **2004**, *20*, 8620–8624.
(40) Lavrich, D. J.; Wetterer, S. M.; Bernasek, S. L.; Scoles, G. *J. Phys. Chem. B* **1998**, *102* (18), 3456–3465.
(41) Rabalais, J. W. Principles and Applications of Ion Scattering Spectrometry. *Surface Chemical and Structural Analysis*; Wiley-Interscience: New York, 2003.
(42) Rodríguez, L. M.; Gayone, J. E.; Sánchez, E. A.; Ascolani, H.; Grizzi, O.; Sánchez, M.; Blum, B.; Benitez, G.; Salvarezza, R. *Surf. Sci.* **2006**, *600*, 2305–2316. Rodríguez, L. M.; Gayone, J. E.; Sánchez, E. A.; Grizzi, O.; Blum, B.; Salvarezza, R. C. *J. Phys. Chem. B* **2006**, *110*, 7095.
(43) Rodríguez, L. M.; Gayone, J. E.; Sánchez, E. A.; Grizzi, O.; Blum, B.; Salvarezza, R. C.; Xi, L.; Lau, W. M. *J. Am. Chem. Soc.* **2007**, *129*, 7807–7813.
(44) Ziegler, J. F.; Ziegler, M. D.; Biersack, J. P. Computer code SRIM 2006.02, 2006; http:/www.srim.org.
(45) McGuiness, C. L.; Blasini, D.; Masejewski, J. P.; Uppili, S.; Cabarcos, O. L.; Smilgies, D.; Allara, D. L. *J. Am. Chem. Soc.* **2006**, *128* (15), 5231–5243.
(46) Zhou, C.; Jones, J. C.; Trionfi, A.; Hsu, J. W. P.; Walker, A. V. *J. Phys. Chem. C* **2009**; DOI: 10.1021/jp905612p.
(47) Adlkofer, K.; Eck, W.; Grunze, M.; Tanaka, M. *J. Phys. Chem. B* **2003**, *107*, 587–591.
(48) McGuiness, C. L.; Shaporenko, A.; Zharnikov, M.; Walker, A. V.; Allara, D. L. *J. Phys. Chem. C* **2007**, *111*, 4226–4234.
(49) Vilan, A.; Ghabboun, J.; Cahen, D. *J. Phys. Chem. B* **2003**, *107*, 6360–6376.
(50) Voznyy, O.; Dubowski, J. J. *Langmuir* **2008**, *24*, 13299–13305.
(51) Yamamoto, H.; Butera, R. A.; Gu, Y.; Waldeck, D. H. *Langmuir* **1999**, *15*, 8640–8644.
(52) Wampler, H. P.; Zemlyanov, D. Y.; Ivanisevic, A. *J. Phys. Chem. Lett.* **2007**, *111*, 17989–17992.
(53) Park, H. H.; Ivanisevic, A. *J. Phys. Chem. C* **2007**, *111*, 3710–3718.
(54) Pruessner, M. W.; Ghodssi, R.; Lim, H.; Carraro, C.; Maboudian, R. *Langmuir* **2004**, *20*, 743–747.
(55) Zerulla, D.; Chasse, T. *Langmuir* **2002**, *18*, 5392–5399.
(56) Gu, Y.; Waldeck, D. H. *J. Phys. Chem. B* **1998**, *102*, 9015–9028.
(57) Yamamoto, H.; Waldeck, D. H. *J. Phys. Chem. B* **2002**, *106*, 7469–7473.
(58) Zerulla, D.; Chassé, T. *J. Electron. Spectrosc. Relat. Phenom.* **2009**, *172*, 78–87.
(59) Jun, Y.; Zhu, X.-Y.; Hsu, J. W. P. *Langmuir* **2006**, *22*, 3627–3632.
(60) Rosu, D. M.; Jones, J. C.; Hsu, J. W. P.; Kavanagh, K. L.; Tsankov, D.; Schade, U.; Esser, N.; Hinrichs, K. *Langmuir* **2009**, *25*, 919–923.
(61) Gayone, J. E.; Pregliasco, R. G.; Gómez, G. R.; Sánchez, E. A.; Grizzi, O. *Phys. Rev. B* **1997**, *56*, 4186.
(62) Gayone, J. E.; Sánchez, E. A.; Grizzi, O. *Surf. Sci.* **1999**, *419*, 188.
(63) Poirier, G. E.; Fitts, W. P.; White, J. M. *Langmuir* **2001**, *17*, 1176.
(64) Vericat, C.; Vela, M. E.; Benitez, G.; Carro, P.; Salvarezza, R. C. *Chem. Crit. Rev.* **2010**, DOI: 10.1039/b907301a.
(65) Serkovic Loli, L. N.; Gayone, J. E.; Martiarena, M. L.; Sánchez, E. A.; Grizzi, O.; Pasquali, L.; Doyle, B.; Nannarone, S.; Hamoudi, H.; Dablemont, C.; Esaulov, V. A. *J. Phys. Chem. C* **2009**, *113*, 17866–17875.

JP1044157